Research in Astronomy and Astrophysics, 25:055002 (11pp), 2025 May
https://doi.org/10.1088/1674-4527/adc789
CSTR: 32081.14.RAA.adc789

Timing and Spectral Analysis of 4U 1626-67 Using AstroSat/LAXPC

N. J. Juris[1], Marykutty James[1], and Jincy Devasia[2]
[1] St.Thomas College, Ranni, Pathanamthitta—689673, India; njjuris@gmail.com
[2] Henry Baker College, Melukavu, Kottayam—686652, India
Received 2024 November 16; revised 2025 March 5; accepted 2025 March 28; published 2025 May 5

Abstract

We present a comprehensive analysis of AstroSat/LAXPC data of the second spin-up and second spin-down phases of the persistent X-ray pulsar 4U 1626-67. Flares followed by a broad dip are detected in the spin-up observations. The pulse profiles changed from a shoulder-like structure to a broad sinusoidal shape as the source underwent a torque reversal from spin-up to spin-down. Energy-resolved pulse profiles in lower energies showed a double-horned profile in the spin-up state and a flat top with multiple peaks in the spin-down state. Regardless of the torque state, the pulse profiles exhibit a broad single-peaked shape at higher energies. The observation in the spin-down era is characterized by the presence of a prominent QPO at 46.5 ± 1.0 mHz frequency. The QPO rms and center frequency show a correlation with energy. Spin-up and spin-down states show a difference in the shape of the power density spectrum. After the torque reversal, a gradual flux drop and the hardening of the spectra were observed. The difference in the shape of the pulse profiles and the presence and absence of QPOs can be explained by the change in accretion flow geometry of the pulsar, from pencil-beam to fan-beam, between spin-down and spin-up states.

Key words: (stars:) pulsars: individual (4U 1626-67) – X-rays: binaries – X-rays: general

1. Introduction

Ultracompact X-ray binaries (UCXBs) are a subgroup of low-mass X-ray binaries (LMXBs) with less than one-hour orbital periods. Since UCXBs have short orbital periods, only an evolved compact donor could fit into such tight orbits (Tutukov & Yungel'Son 1993; Deloye et al. 2005). The evolved UCXB donors are most likely anticipated to be hydrogen-deficient (Paczynski & Sienkiewicz 1981). The persistent LMXB pulsar 4U 1626-67 is classified as a UCXB due to its 42 minute orbital period. This accreting X-ray pulsar located at a distance of ∼5–13 kpc from the Sun (Chakrabarty 1998) has a very low mass companion, with the estimated mass in the ∼0.03–0.09 $M_{\odot}$ range (Levine et al. 1988). It was discovered with the Uhuru satellite (Giacconi et al. 1972), and X-ray pulsations with a period of ∼7.7 s were identified with SAS-3 observations by Rappaport et al. (1977).

Since its discovery, the persistent X-ray source 4U 1626-67 has experienced three torque reversals (Camero-Arranz et al. 2010; Sharma et al. 2023). It was initially observed in a spin-up state and began to spin down in 1990 following a torque reversal. In 2008, a transition occurred from a consistent spin-down phase that lasted almost 18 yr to a spin-up phase (Benli 2020). Again, it underwent a recent torque reversal in 2023 after 15 yr of spin-up phase (Sharma et al. 2023). The torque reversal is accompanied by changes in the luminosity of 4U 1626–67. The transition from the first spin-up state to the first spin-down state witnessed a decrease in the X-ray flux (Chakrabarty et al. 1997). The second torque reversal to the spin-up phase was accompanied by an increase in the source luminosity about two to three times (Jain et al. 2010). In 2010, two years following that torque reversal, the source's X-ray flux reached almost the same level as in 1977 (Camero-Arranz et al. 2010). The recent shift to a spin-down state in 2023 was accompanied by a decrease in the luminosity of the source, similar to the first detected phase transition (Jenke et al. 2023; Sharma et al. 2023).

Both X-ray and optical flares have been observed in this LMXB pulsar since the earliest observations (McClintock et al. 1980), with detections continuing consistently over the following years (Raman et al. 2016; Beri et al. 2018). 4U 1626-67 shows strong flaring activity with a duration of a few hundred seconds during the spin-up state and comparatively fewer flares in the spin-down state (Chakrabarty et al. 2001; Beri et al. 2014). X-ray flares of different durations and recurrence times have been previously reported in many other sources like 4U 1901+03 (James et al. 2011), SMC X-1, and LMC X-4 (Moon et al. 2003a, 2003b). The X-ray characteristics of 4U 1626-67 differ in spin-up and spin-down phases. A notable difference is the disappearance of the bi-horned peaks observed in the low-energy pulse profiles during the spin-up state, from the profiles of the spin-down state (Beri et al. 2014, 2018).

Quasi-Periodic Oscillations (QPOs) in the power spectrum of accretion-powered X-ray pulsars are believed to arise due to

inhomogeneities in the inner accretion disk and are considered as an important signature of the presence of an accretion disk. During the spin-down eras of 4U 1626-67, observations revealed prominent QPOs around 48 mHz, displaying a gradual evolution in frequency over time (Chakrabarty 1998). In the first spin-down phase, QPOs at 48 mHz were consistently observed across all observations, while these QPOs were absent during the following spin-up phase (Kaur et al. 2008; Jain et al. 2010). However, weak and broad QPOs around 40 mHz were identified in the initial spin-up phase from Ginga observations, indicating variations in QPO characteristics between spin-up and spin-down states (Shinoda et al. 1990). These aperiodic variabilities are detected in several other X-ray sources including KS 1947+300 (James et al. 2010), LMC X-4 (Moon & Eikenberry 2001), and Cen X-3 (Raichur & Paul 2008).

The spectrum of 4U 1626-67 has been extensively studied using data from various observatories, revealing a two-component structure composed of a blackbody and a power law (Pravdo et al. 1979; Kii et al. 1986; Krauss et al. 2007; Camero-Arranz et al. 2012). These continuum spectral parameters have been observed to vary during periods of torque reversal. The spectrum had a blackbody temperature of around 0.6 keV and a power-law photon index (PI) of about 1.5 in the first spin-up state (Pravdo et al. 1979; Kii et al. 1986). The blackbody temperature dropped to about 0.3 keV during the first spin-down state, and the energy spectrum became comparatively harder with a power-law index of 0.4–0.6 (Angelini et al. 1995; Orlandini et al. 1998). Similar to the first spin-up state, the second spin-up phase showed a higher blackbody temperature of roughly 0.5–0.6 keV but the PI did not go back to the previous range and showed values near 0.8–1.0 (Krauss et al. 2007; Camero-Arranz et al. 2010; Jain et al. 2010). Additionally, numerous spectroscopic observations have reported unusually bright emission lines of neon (Ne) and oxygen (O) (Krauss et al. 2007; Camero-Arranz et al. 2010). The surface magnetic field of 4U 1626-67 is estimated to be approximately $\sim 3 \times 10^{12}$ Gauss, based on the detection of a cyclotron line feature around 37 keV in its spectra, observed across multiple observatories during both spin-up and spin-down states (Pravdo et al. 1979; Orlandini et al. 1998; Camero-Arranz et al. 2010).

This work includes the timing and spectral analysis of the X-ray binary 4U 1626-67 utilizing data from Large Area X-ray Proportional Counter (LAXPC) onboard AstroSat for the first time. We have analyzed the LAXPC20 observations of this source from 2016 January to 2023 May. The observations and data analysis are described in Section 2 and timing analysis is carried out in Section 3.1. The pulse profiles and QPO are studied in detail in Sections 3.1.2 and 3.1.3. 3.2 describes spectral analysis followed by discussions and conclusions in Section 4.

Table 1
Details of AstroSat/LAXPC Observations of 4U 1626-67 from different Epochs

Data	Obs. ID	Observation Date	No. of Orbits	Exposure Time (ks)
Data1	G02_020T02_9000000268	2016 Jan 13	4	8.21
Data2	G02_020T02_9000000294	2016 Jan 26	5	12.19
Data3	G05_021T01_9000000624	2016 Aug 26	12	41.69
Data4	G07_049T01_9000001352	2017 Jul 2	21	67.85
Data5	G08_084T01_9000002100	2018 May 15	23	36.35
Data6	T05_106T01_9000005642	2023 May 18	21	42.06

2. Observations and Data Analysis

AstroSat, the first multi-wavelength astronomical satellite from India, was launched in 2015 (Singh et al. 2014). Its five payloads are the LAXPC, Cadmium-Zinc-Telluride Imager (CZTI), Soft X-ray Telescope (SXT), Ultraviolet Imaging Telescope (UVIT), and Scanning Sky Monitor (SSM). The LAXPC is composed of three detectors, the LAXPC10, LAXPC20, and LAXPC30. LAXPC operates in the energy range of 3–80 keV with a 6000 cm^2 area and 10 ms time resolution. It operates in two modes: Broad Band Counting and Event Mode. This work uses the event mode data as it records the energy, identity, and arrival time of each event (Yadav et al. 2016).

AstroSat made several observations of 4U 1626–67 between 2016 January and 2023 May. The observations were downloaded from the Indian Space Science Data Centre (ISSDC) archive[3] and the observational details are given in Table 1. In this work, we limit our research to data from LAXPC20 as the LAXPC30 detector is not working and LAXPC10 exhibits gain variation and gas leakage. For LAXPC data analysis, we used the tools available in LAXPCSoft V3.4.4 developed at TIFR/IUCAA.[4] Spectral analysis was done using the XSPEC version 12.11.1 available in HEASOFT [5] version 6.28.

The LAXPC level-1 data are processed to extract events, light curves, spectra, and background files for the Good Time Intervals (GTI). The LAXPC pipeline software runs by taking the required input files from its well-defined directory structure, which includes level-1 data files, calibration, and background files for the generation of level-2 data products. The required background files are supplied along with the software. The software itself offers guidance for the selection of a suitable background as well as a response file that may be used for further analysis (Mukerjee & Antia 2021). The pipeline generates background-subtracted light curves and calibrated spectra for further analysis of the source. Light curves were

[3] https://www.issdc.gov.in/astro.html
[4] https://www.tifr.res.in/astrosat_laxpc/LaxpcSoft.html
[5] https://heasarc.gsfc.nasa.gov/docs/software/lheasoft/download.html

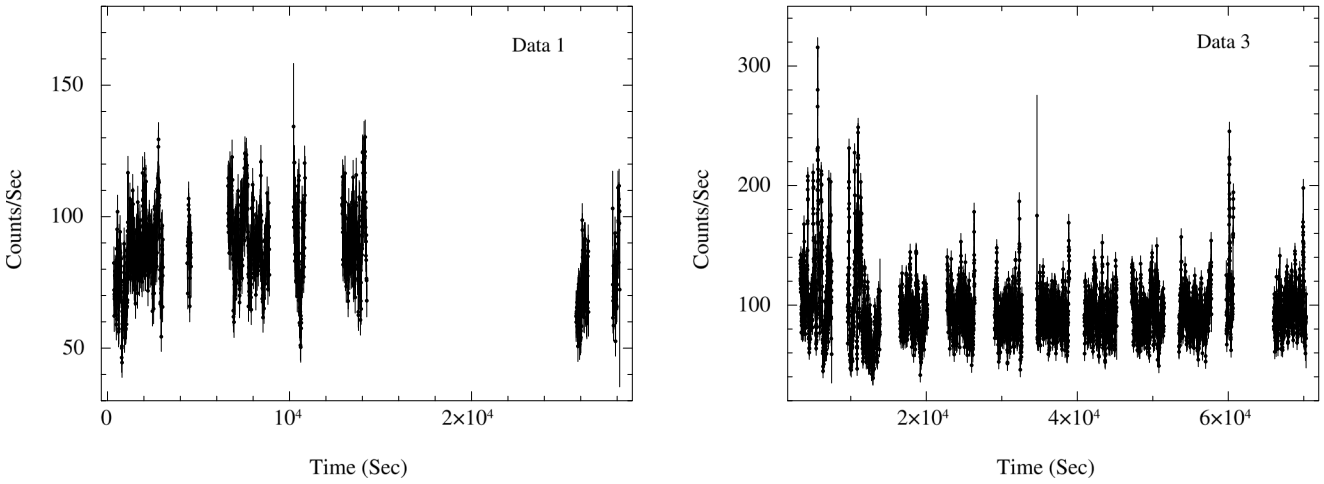

Figure 1. The 3–80 keV background-subtracted light curves of 4U 1626-67 from LAXPC observations of 2016 January (left) and 2016 August (right).

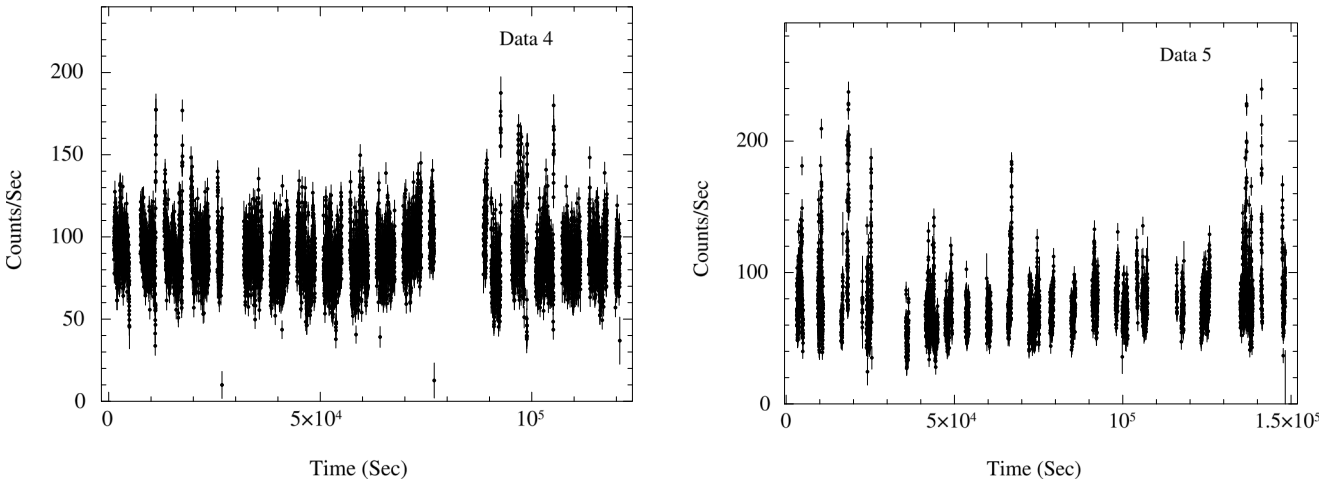

Figure 2. The 3–80 keV background-subtracted light curves of 4U 1626-67 from LAXPC observations of 2017 July (left) and 2018 May (right).

corrected to the solar system barycenter using *barycorr*[6] by HEASOFT.

3. Results

3.1. Timing Analysis

3.1.1. Light Curves

We created 3–80 keV background-subtracted light curves using the main anodes and all layers of LAXPC20 for a bin size of 0.01 s. The source has a persistent count rate of $\sim$100 c s^{-1} in Data 1 to Data 5 when it was in the spin-up state. The average intensity of the source seems to have been reduced to $\sim$30 c s^{-1} in Data 6 when the source returned to spin-down. The light curves of Data 3, Data 4, and Data 5 show the presence of flares. These flares have an intensity two or more times greater than the quiescent level and are 100–300 s long. They have a symmetric shape with steady rise and decay and reoccur with timescales varying between 300 s and 700 s. The flares of 4U 1626-67 in the spin-up state of our observations show energy dependence and are visible up to $\sim$15 keV in the light curves. In the Data 3 light curve, two flares are seen together with $\sim$100 s separation; the first one is the largest flare among all the observations analyzed in this work. The first and second flares have their intensity rising above $\sim$3 and $\sim$2 times the quiescent level, respectively. A broad dip reducing in intensity to below the persistent level was observed after the decay of the second flare at 6200 s in Figure 1 (right panel). This dip in the intensity recovered to the persistent level after $\sim$250 s and is depicted in Figure 3 (right panel). The barycenter-corrected light curves of all the observations with a bin size of 7.7 s are displayed in Figures 1, 2, 3 and 4. The left

[6] https://heasarc.gsfc.nasa.gov/docs/software/heasoft/help/barycorr.html

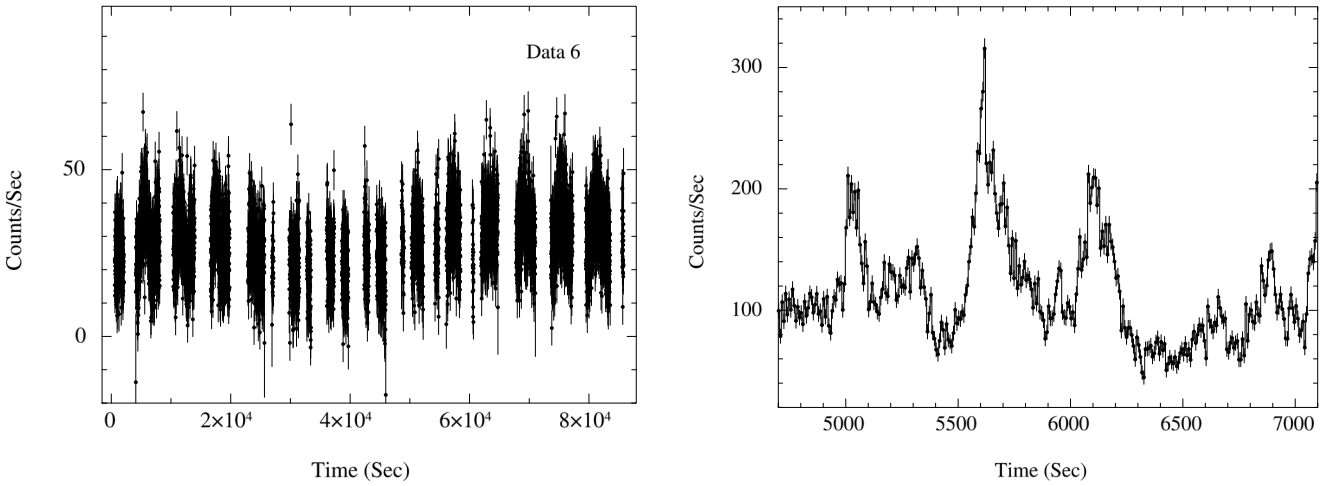

Figure 3. The 3–80 keV background-subtracted light curve of 4U 1626-67 from LAXPC observations of 2023 May (left) and the rescaled light curve of Data 3, showing the region with consecutive flares and the subsequent dip (right).

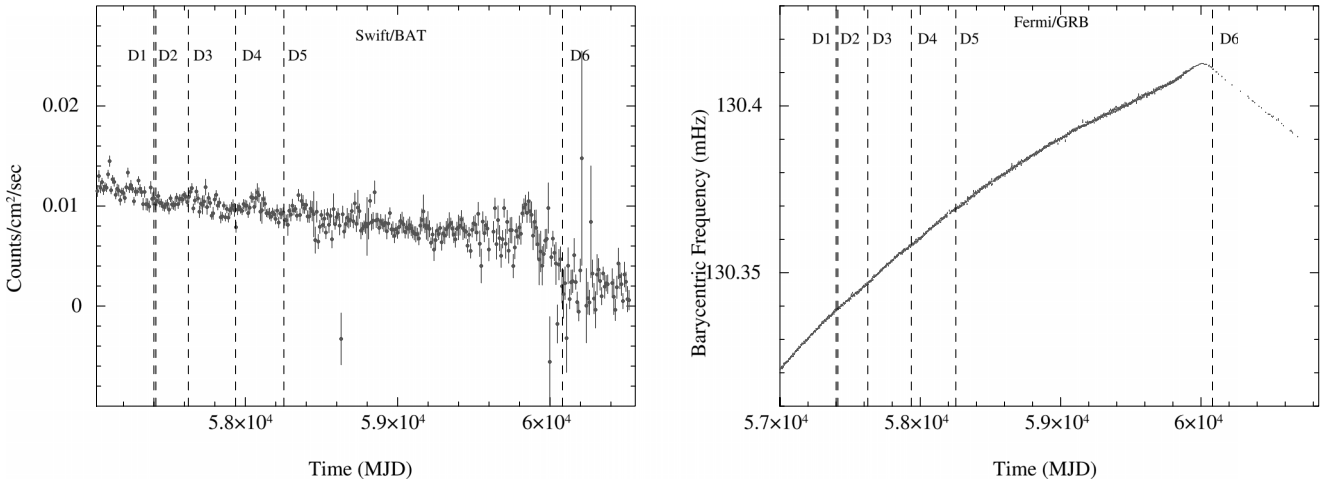

Figure 4. The Swift-BAT light curve of 4U 1626-67 in the 15–50 keV range, binned to 10 days (left) and the Fermi-GBM spin history of 4U 1626-67 (right). Vertical dashed lines on both plots signify the LAXPC20 observations.

panel of Figure 4 shows the positions of LAXPC20 observations in the Swift- BAT light curve of 4U 1626-67, and the right panel shows the Fermi-Gamma-ray Burst Monitor (GBM) spin history of 4U 1626-67.

3.1.2. Pulse Profile

Using the FTOOLS task EFSEARCH, we applied the χ^2 maximization method and pulse folding to obtain the spin period. Spin periods of 7.6723 s, 7.6723 s, 7.6718 s, 7.6712 s, 7.6705 s, and 7.6681 s were obtained respectively for Data 1, Data 2, Data 3, Data 4, Data 5, and Data 6. The 3–80 keV light curves were folded at the respective spin periods. The pulse profile of Data 2 is distorted and has very few statistics, thus it is omitted from analysis. Energy average pulse profiles with 64 phase bins created for all other observations are plotted in Figure 5. The 3–80 keV pulse profile of Data 1 to 5 exhibits a main peak and two steps on both sides (a shoulder-like structure). The small step before the main peak is of lesser amplitude than the following step. In Data 1, a significant dip in the intensity is observed before the main peak; which diminishes in the subsequent observations. The small peak after the main peak broadens and eventually joins with the latter, as the source evolves in the spin-up state. The shift from spin-up to spin-down, between data 5 and data 6, of the source is characterized by the change in the shape of the energy-averaged pulse profile to a broad sinusoid with many spikes.

4U 1626-67 is known to show strong energy-dependent pulse profiles. We created pulse profiles using the light curves in the

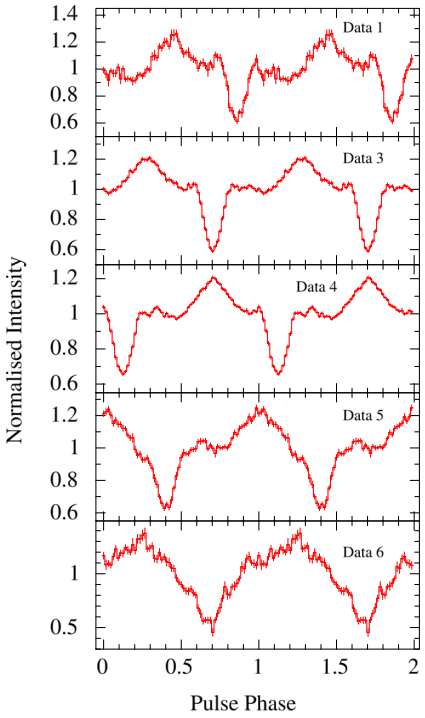

Figure 5. The 3–80 keV pulse profiles of 4U 1626-67 generated from observations made with AstroSat/LAXPC. The folded light curves are normalized to counts s^{-1}.

energy bands of 3–6 keV, 6–9 keV, 9–12 keV, 12–15 keV, 15–18 keV, 18–21 keV, 21–24 keV and 24–52 keV. We could detect pulsations only up to 52 keV, but above that, pulsations were undetectable due to poor statistics in the data. These energy-dependent pulse profiles of all the observations are plotted in Figures 6, 7 and 8.

The pulse profile during the spin-up state (Figures 6 and 7) shows a double-horned pulse shape separated by a narrow dip, in the low energies and a single-peaked profile in higher energies. In the lower energy bands up to 9 keV, a sharp double-peak is observed, with the first peak being greater in amplitude than the second peak except in the case of Data 5 (Figure 7 right panel) where the second peak is of greater amplitude. With increasing energy, the narrow dip between the two peaks broadens. The phase before and after the double-peaks is characterized by the presence of a broad minimum, which disappears as the profile evolves in energy. Above 9 keV, a small peak appears just before the first peak and increases in intensity. No double-horned structure is observed above 18 keV, resulting in the shape change of the profile to a single-peaked pulse.

After the torque reversal, the pulse profiles changed in morphology to a flat top with many small peaks in the lower energies and a broad sinusoid in the higher energies as affirmed in Figure 8. The 3–6 energy band shows a flat broad profile with multiple small peaks. The shape slightly shifts to a broad

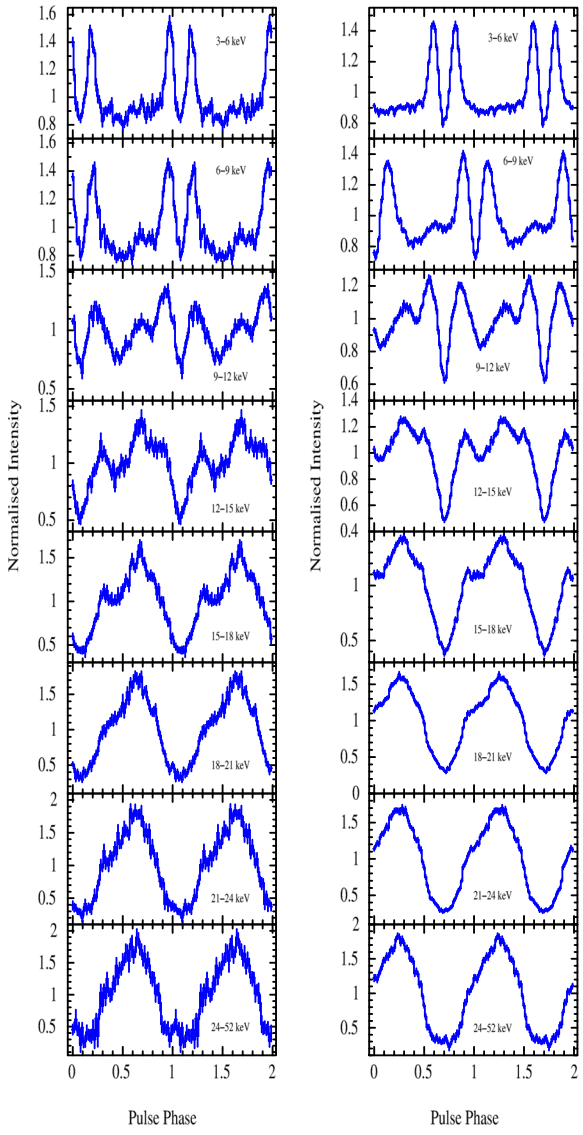

Figure 6. Energy resolved pulse profile of Data 1 (left), and Data 3 (right) of 4U 1626-67 generated from observations made with AstroSat/LAXPC.

single peak in the following energies. Above 18 keV, the pulse profile has a broad sinusoidal shape with many spikes on it. The pulse fraction (PF), which is expressed by the relation $\mathrm{PF} = \frac{P_{\max} - P_{\min}}{P_{\max} + P_{\min}}$, represents the relative amplitude of the changing pulse profile. The PFs for Data 1, Data 3, Data 4, Data 5, and Data 6 are 34.8% ± 1.6%, 34.4% ± 0.9%, 29.6% ± 0.6%, 33.3% ± 1.1% and 50.5% ± 3.3%, respectively. It may be noted that there is a statistically significant increase in the value of PF as the source underwent torque reversal. While a single observation is not sufficient to definitively conclude this, the observed trend suggests an increase in PF as the source underwent a torque reversal from spin-up to spin-down. This trend aligns with previous studies

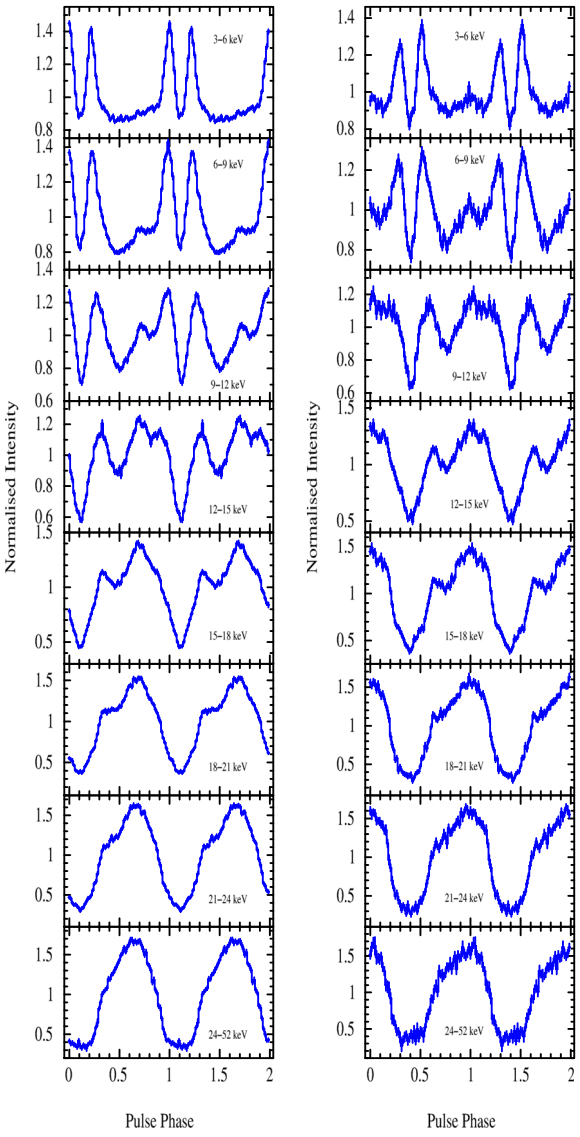

Figure 7. Energy resolved pulse profile of Data 4 (left), and Data 5 (right) of 4U 1626-67 generated from observations made with AstroSat/LAXPC.

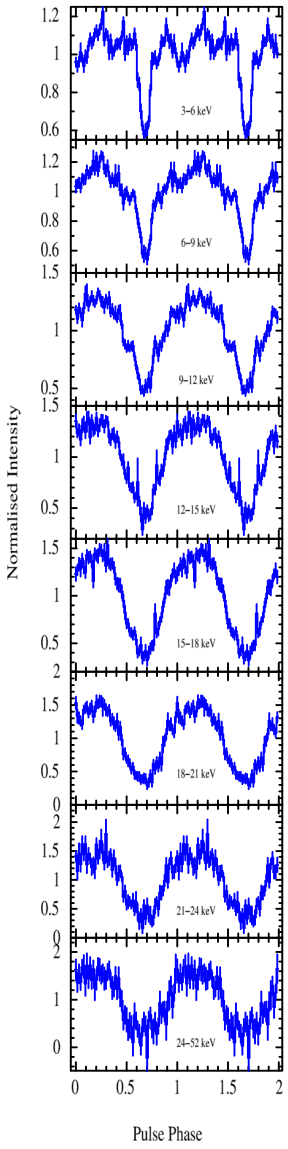

Figure 8. Energy resolved pulse profile of Data 6 of 4U 1626-67 generated from observations made with AstroSat/LAXPC.

of the source, which have reported similar behavior during torque reversals (Beri et al. 2014; Sharma et al. 2023).

3.1.3. Power Density Spectra

The Power Density Spectrum (PDS) was created using the FTOOL POWSPEC for each data set to search for any aperiodic variability. The PDS was made for small data segments of 8192 s, and approximately six intervals were averaged into a single frame to improve the detectability of the QPO-like features. The PDS was normalized (norm $= -2$) such that its integral gives the squared rms fractional variability, and the white noise level is subtracted.

We have noticed a change in the shape of the PDS of our observations between the spin-up and spin-down states. Data 1 to Data 5 exhibited an inclined-shaped continuum with a broad bump around the $\sim$2 mHz frequency. This broad feature was energy-dependent and distinguishable up to $\sim$21 keV. Additionally, a broadening of the spin frequency peak was evident in the PDS of Data 3, Data 4, and Data 5. However, as the source transitioned into the spin-down phase following a torque reversal, the PDS continuum flattened, and both the broad feature at low frequencies and the broadening of the spin frequency peak disappeared. Notably, during the spin-down state (Data 6), a prominent QPO-like feature at 46.5 ± 1.0 mHz was detected. The same attribute has been identified with a NuSTAR observation of the source during 2023 May by

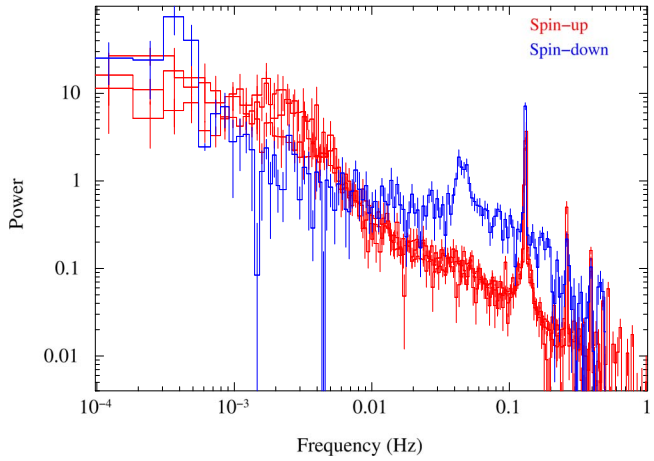

Figure 9. The 3–80 keV PDS of 4U 1626-67 from AstroSat/LAXPC observations of both the spin-up and the spin-down states.

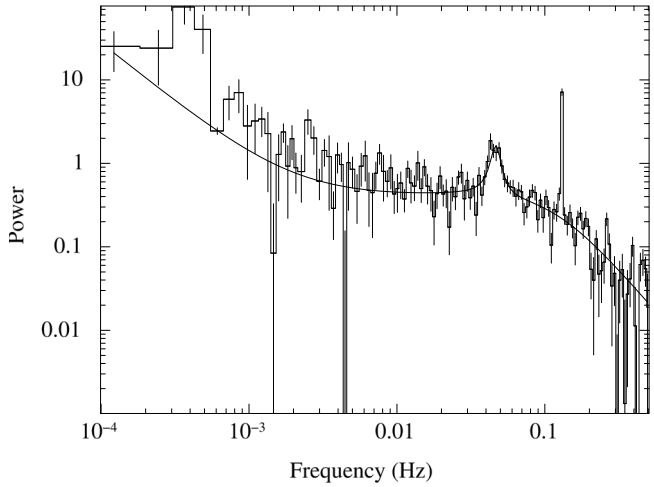

Figure 10. The PDS of 4U 1626-67 from AstroSat/LAXPC observation of Data 6 fitted with a power law and two Lorentzians.

Sharma et al. (2023). The QPO feature in the PDS could be detected up to ∼15 keV. The PDS of spin-up states (in red) and spin-down states (in blue) are overlaid and plotted in Figure 9 for comparison.

The continuum of the power spectrum of Data 6 was fitted with a model consisting of a power-law component with a PI of 1.03 and a Lorentzian with a Lorentzian Center (LC) of 0.2 Hz. The QPO feature was fitted by adding another Lorentzian with the value of LC around 0.045 Hz. The fitted PDS is shown in Figure 10. The quality factor of the QPO is about 2.96, and the QPO significance is 3.7σ. The rms fractional variability calculated from the background-subtracted data is 11.94% ± 3.2%. The center frequency of the QPO is found to be 46.5 ± 1.0 mHz, and the QPO feature has a width of about 7.76 ± 2.3 mHz. The left panel of Figure 11 presents the energy dependence of the rms value of the QPO. While significant uncertainties in the results limit definitive conclusions, the observed positive correlation between rms value and energy is consistent with previous studies of the source (Manikantan et al. 2024). The change in QPO center frequency with energy is studied and the plot is displayed on the right panel of Figure 11. The center frequency is observed to increase up to approximately 8 keV, beyond which it exhibits a decrease. We could not check the time evolution of the QPO frequency as the available data are insufficient for such an analysis.

3.2. Spectral Analysis

We used XSPEC version 12.12.1 for the spectral fitting. We analyzed the 3.0–20.0 keV spectra from four of the six LAXPC20 observations. Data 1 and 2 have very little exposure time and thus poor statistics, leading to the exclusion of the spectra of those observations from further analysis.

In analyzing the spectra of Data 3 to Data 5, we used the spectral model with a power law and blackbody. The absorption component was introduced by the model TBABS,[7] which describes the X-ray absorption by the interstellar medium (ISM). The absorption column density (n_H) value is fixed at $9.52 \times 10^{20}\,\mathrm{cm}^{-2}$, as given by HI4PI Collaboration et al. (2016). We did not detect any difference in the parameters of the blackbody component with or without freezing the hydrogen column density. Adding a Gaussian at the broad iron emission line that was detected improved the fit and reduced the value of $\Delta\chi^2$. The iron line energies obtained in our results are higher than those reported by Tobrej et al. (2024) and Sharma et al. (2023). This discrepancy could be due to the lower spectral resolution (FWHM 1.2 keV at 6 keV) of LAXPC (Antia et al. 2017).

The final used spectral model is *tbabs* ∗ (*powerlaw* + *bbody* + *Gaussian*). The spectral uncertainties of the parameter values are computed using the *error* command, to 90% confidence level. The detected value of the PI was around 0.96. The blackbody temperature varied between 0.62 and 0.68 keV. The observed flux value is decreasing over the years from $6.18 \times 10^{-10}\,\mathrm{erg\,cm^{-2}\,s^{-1}}$ in 2016 August to $5.54 \times 10^{-10}\,\mathrm{erg\,cm^{-2}\,s^{-1}}$ in 2017 July to $4.81 \times 10^{-10}\,\mathrm{erg\,cm^{-2}\,s^{-1}}$ in 2018 May. For all these spin-up state observations, the reduced chi-square values are lower than 1. However, the results remain consistent with previous studies (Beri et al. 2014, 2018; Sharma et al. 2023; Tobrej et al. 2024).

A spectral model with power law and blackbody is used to fit the Data 6 spectrum. We also used the *gain* command in XSPEC to account for the uncertainty in the gain of the LAXPC20 detector. Even though no significant iron emission line was detected, a broad feature around ∼7 keV is seen in the spectra. However the addition of a Gaussian did not improve

[7] https://heasarc.gsfc.nasa.gov/xanadu/xspec/manual/node268.html

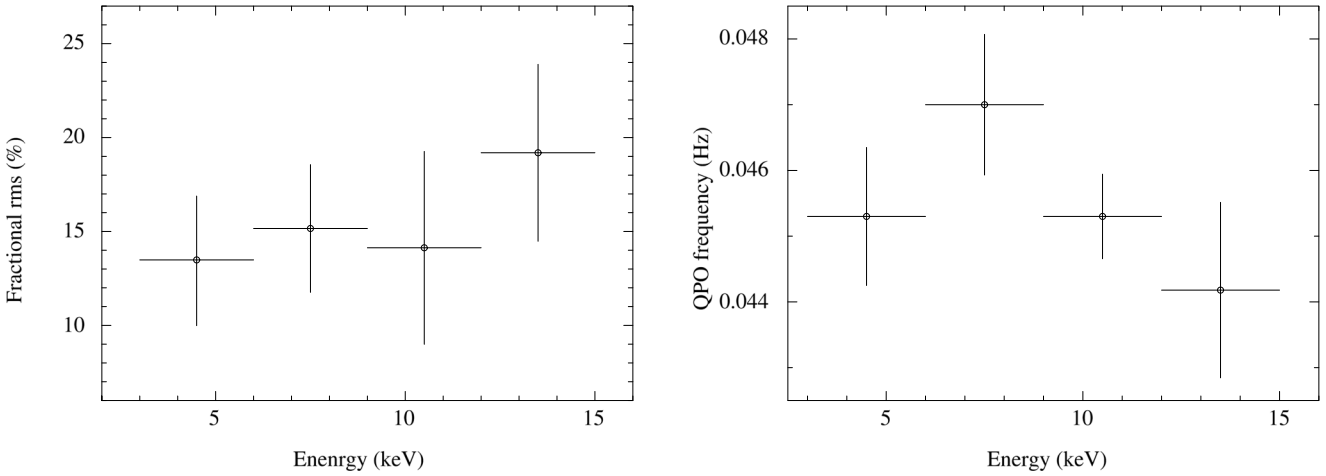

Figure 11. The energy-dependent variation of QPO fractional rms amplitude (left) and QPO center frequency (right) of 4U 1626-67 from AstroSat/LAXPC observations.

Table 2
Best-fitting Parameters of the Spectra of 4U 1626-67 from Data 3 to Data 6

Parameter	Data 3	Data 4	Data 5	Data 6
PhoIndex (Γ)	$0.99^{+0.04}_{-0.05}$	0.95 ± 0.05	$0.96^{+0.04}_{-0.05}$	$0.85^{+0.19}_{-0.25}$
$\mathrm{Norm_{PL}}$	$2.1 \pm 0.2 \times 10^{-2}$	$1.7 \pm 0.2 \times 10^{-2}$	$1.5^{+0.1}_{-0.2} \times 10^{-2}$	$2.83^{+1.9}_{-1.5} \times 10^{-3}$
$\mathrm{kT_{Bbody}}$ (keV)	$0.628^{+0.22}_{-0.24}$	$0.68^{+0.17}_{-0.2}$	$0.66^{+0.16}_{-0.15}$	$2.24^{+0.12}_{-0.08}$
$\mathrm{Norm_{Bbody}}$	$9.78 \pm 4.0 \times 10^{-4}$	$8.16^{+9.0}_{-2.0} \times 10^{-4}$	$6.22^{+5.2}_{-2.0} \times 10^{-4}$	$8.81^{+1.9}_{-1.7} \times 10^{-4}$
LineE (keV)	$7.26^{+0.54}_{-1.39}$	$7.2^{+0.5}_{-1.2}$	$7.37^{+0.36}_{-0.65}$	...
Sigma (keV)	$1.0^{+1.03}_{-0.71}$	$1.23^{+0.87}_{-0.57}$	$0.92^{+0.76}_{-0.59}$	...
Eqw (keV)	$0.29^{+0.26}_{-0.21}$	$0.44^{+0.45}_{-0.43}$	$0.32^{+0.33}_{-0.31}$	...
$\mathrm{Norm_{Gaus}}$	$8.86^{+1.4}_{-4.0} \times 10^{-4}$	$11.6^{15.7}_{-5.6} \times 10^{-4}$	$7.47^{+7.7}_{-3.4} \times 10^{-4}$	...
Flux (erg $\mathrm{cm^{-2}\,s^{-1}}$)	$6.18^{+0}_{-0} \times 10^{-10}$	$5.54^{+0}_{-0} \times 10^{-10}$	$4.81^{+0}_{-0} \times 10^{-10}$	$1.75^{+0}_{-0} \times 10^{-10}$
χ^2/ dof	14.28/21	15.08/23	14.68/23	21.62/24

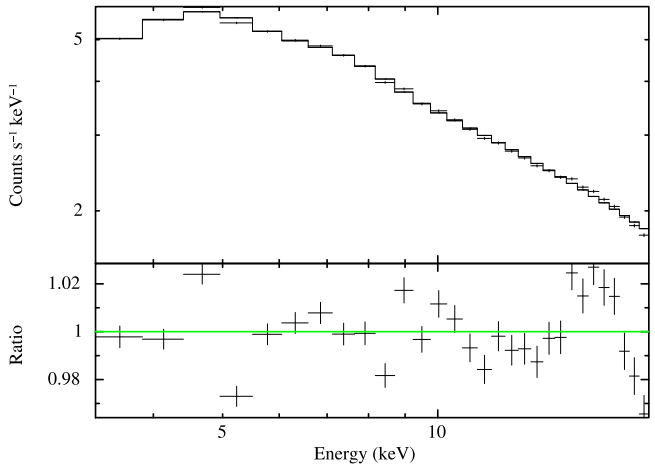

Figure 12. The best-fit spectrum and ratio of Data 5 to the model *tbabs* $*$ (*powerlaw* + *bbody* + *Gaussian*) from AstroSat/LAXPC observation of 4U 1626-67.

$\Delta\chi^2$, so we used the model *tbabs* $*$ (*powerlaw* + *bbody*) for the spectral fit. The value of the PI lowered to 0.85 and the blackbody temperature changed to 2.24 keV. The flux value also decreased to 1.75×10^{-10} erg $\mathrm{cm^{-2}\,s^{-1}}$. The best-fitting spectrum of the 2018 May observation is shown in Figure 12 and the best-fitting parameters of all the spectral observations are given in Table 2.

4. Discussion

This work reports results of the timing and spectral analysis of the persistent pulsar 4U 1626-67 during its spin-up and spin-down states from 2016 January to 2023 May, using AstroSat/LAXPC observations. Since its discovery, this source has experienced multiple torque reversals, including a transition from spin-up to spin-down in 1990, spin-down to spin-up in 2008, and a return to spin-down in 2023. Such torque reversals

are observed in a few other sources like GX 1+4, Cen X-3, and Her X-1 (Bildsten et al. 1997). Among these, GX 1+4 and 4U 1626-67 have maintained decades-long torque states with steady spin-up and steady spin-down (Perna et al. 2006).

A distinctive feature of the LMXB pulsar 4U 1626-67 is the presence of flares in its light curve, which are generally observed during periods of spin-up (Joss et al. 1978; Beri et al. 2014, 2018). We detected strong flares, with intensity reaching two to three times that of the quiescent level, in the light curve when the source was in its second spin-up era. Flares with similar characteristics have been previously observed in this state in X-ray data (Beri et al. 2014, 2018; Schulz et al. 2019) and in optical data (Raman et al. 2016). The flares observed in our results exhibit a symmetric rise and decay, followed by a dip in persistent emission. This behavior is similar to the Type II bursts in GRO J1744-28, which showed the presence of a dip and a recovery period following each outburst (Giles et al. 1996). The Lightman-Eardley (LE) instability (Lightman & Eardley 1974) is suggested to be the dominant mechanism behind the Type II bursts in GRO J1744-28 (Li & van den Heuvel 1997; Cannizzo 1996). The LE instability arises when the radiation pressure in the inner accretion disk becomes comparable to the gas pressure, and the material that is evacuated onto the pulsar during an accretion event is replenished by material flowing in from further out. This causes the dip and recovery in the light curve following an outburst (Cannizzo 1996). The presence of a dip following the two consecutive flares in Data 3 of our observation points to the possibility that an accretion instability-potentially the LE instability-contributes to the flaring behavior of 4U 1626-67. Previous XMM-Newton (Beri et al. 2018) and Chandra (Schulz et al. 2019) observations of the source during its second spin-up phase also report dips following strong flares. Notably, Beri et al. (2018) also suggested that the LE instability could be responsible for these events. In our observation of Data 6, no flaring activity was detected, consistent with previous reports of minimal flaring during spin-down periods. This absence of flares may be due to localized instabilities within the accretion disk being absent or less pronounced due to the lower accretion rates during spin-down.

Consistent pulsations at $\sim$7.67 s were detected in all the AstroSat/LAXPC observations carried out in this work, during both torque states. Among these, Data 6 were characterized by the presence of a 46.5 $\pm$ 1.0 mHz QPO. We could detect the QPO feature up to $\sim$15 keV. QPOs around 46 and 48 mHz have been detected in the X-ray emission from 4U 1626-67 (Kommers et al. 1998; Chakrabarty et al. 2001; Manikantan et al. 2024) in the spin-down eras and weak $\sim$40 mHz QPOs have been detected during the initial spin-up phase (Shinoda et al. 1990). The presence of QPOs typically during the spin-down state indicates changes in the source's accretion flow geometry with the torque reversal. It can be explained by assuming that QPOs are a manifestation of clumps in the inner accretion disk (Beri et al. 2014).

QPOs are usually detected in the 10–25 keV energy range in accretion-powered pulsars (Raichur & Paul 2008; James et al. 2010), with a notable difference in the case of GX 304-1 in which a QPO feature is seen up to 40 keV (Devasia et al. 2011b). The energy dependence of the QPO center frequency and fractional rms of the QPO are examined. The center frequency increases, peaking within the 3-9 keV energy range before declining. While the fractional rms exhibits a positive trend, we cannot make a definitive conclusion due to the large associated uncertainties. The correlation of QPO rms with energy in 4U 1626-67 was previously observed by Manikantan et al. (2024). The observed positive correlation of the fractional rms amplitude with energy could offer valuable insights into the physical mechanisms driving the QPOs. Studies by Gilfanov et al. (2003) and Mukherjee & Bhattacharyya (2012) suggest that these oscillations may be due to the temperature fluctuations in a blackbody-like component.

The Keplerian frequency of the QPO is determined to be $\nu_k = \nu_{\rm spin} + \nu_{\rm QPO} \approx 0.17$ mHz using the beat frequency model (BFM). BFM suggests that QPOs arise at the beat frequency between the neutron star's spin frequency and the Keplerian frequency at the Alfvén radius of the disk-magnetosphere (Alpar & Shaham 1985). This provides a consistent way to measure the magnetic dipole moment. The magnetic field strength of the pulsar can be approximated by the relation $B_{12} \sim 5.56 \sqrt{L_{37}}$ (Shinoda et al. 1990). This measurement yields an estimate for the magnetic field strength of $\sim 2.55 \times 10^{12}$ Gauss. Previous studies have detected a Cyclotron Resonance Scattering Feature (CRSF) in the spectrum of this pulsar (Orlandini et al. 1998), indicating a surface magnetic field strength of $\sim 3 \times 10^{12}$ Gauss. The magnetic field strength obtained from our study is within a reasonable range of this.

Our spin-up observations, which include detected flares, reveal an energy-dependent broad feature around $\sim$2 mHz in the PDSs. Previous studies have reported QPO−like features around $\sim$3 mHz in the PDS generated from X-ray (Joss et al. 1978; Beri et al. 2018) and optical (Raman et al. 2016) data during previous spin-up states of this source. These studies suggest that such low-frequency features might be associated with the presence of flares during those observations. Although flares are evident in our observations, we cannot conclusively attribute the $\sim$2 mHz feature to them, as interpreting this feature with certainty is challenging due to its frequency being close to the harmonics of AstroSat's orbital frequency ($\sim$0.15 mHz) (Antia et al. 2021).

The broadening in the wings of the pulse frequency peak is observed during the spin-up state. This can be assumed to be due to the coupling between the periodic and aperiodic variabilities in the power spectra (Burderi et al. 1993). It is

also interesting to note that the broadening of the spin-frequency peak is not observed in the PDS where QPO is detected. The disappearance of the broadening during the presence of QPO has been previously reported in 4U 1901+03 by James et al. (2011).

A change in the shape of the PDSs is noticed as the source underwent a torque reversal. Torque reversals in disk-fed X-ray pulsars can plausibly be explained by the warping of the inner accretion disk, which may produce a retrograde disk flow close to the accreting neutron star (van Kerkwijk et al. 1998). Accretion from the inner disk to the neutron star surface likely occurs in different modes that are steady over a long time. Transitions between such stable accretion states that have different accretion flow geometry can result in different X-ray spectra and pulse characteristics (van Kerkwijk et al. 1998). This might be the explanation behind the observed differences in pulse profile, spectra and PDSs between the spin-up and spin-down states of 4U 1626-67.

The pulse profiles' energy and torque state dependency are seen in all the observations analyzed in this work. In the spin-up state, the double-horned profile shifts to a single-peaked profile between lower ($<$12 keV) and higher ($>$18 keV) energies while the energy-averaged pulse profiles show a shoulder-like structure. The low energy profile structures are consistent with those seen in the spin-up eras of the pulsar in previous studies (Beri et al. 2014; Iwakiri et al. 2019). After the torque reversal, the pulse profiles in lower energies ($<$9 keV) show a flat top with multiple small peaks. Such profiles are obtained in the 2–12 keV energy range of the 2003 August XMM-Newton observation (Koliopanos & Gilfanov 2016) when the source was in its spin-down state. Higher energy ($>$15 keV) profiles have a broad sinusoidal structure with narrow spikes similar to the $>$18 keV profiles of the spin-up state. The energy-averaged pulse profile in the spin-down state has a broad sinusoidal shape with many spikes, consistent with the previously reported observations (Angelini et al. 1995; Krauss et al. 2007; Beri et al. 2014).

The difference in the shape of the pulse profile between spin-down and spin-up states can be explained using the change in the accretion flow geometry. The emission diagram of the accretion column depends on the mass accretion rate, transitioning between pencil-beam and fan-beam emission (Basko & Sunyaev 1975). During the spin-down state, when the mass accretion rate is low, the inflowing material is irregular, forming a less stable, narrow accretion column (Iwakiri et al. 2019). This results in emission from the polar hot spots concentrated along the magnetic field axis and directed away from the accretion disk, leading to a pencil-beam emission pattern. Such a configuration is typically associated with single-peaked pulse profiles, though gravitational effects and various obscuration mechanisms can introduce more complex shapes (Meszaros 1992).

When the mass accretion rate is high (spin-up state), the accretion column becomes filled with high-density plasma that slowly sinks under the neutron star's gravitational field. This increases opacity along the magnetic field axis, causing most X-ray photons to escape through the optically thin sides of the accretion column, with the emission directed parallel to the accretion disk, forming a fan-beam pattern (Koliopanos & Gilfanov 2016). This accounts for the narrow dips observed between the double peaks in the low-energy pulse profiles of the spin-up era (White et al. 1983; Rea et al. 2004). Energy-dependent dips in pulse profiles have been observed in numerous X-ray pulsars, with these features being particularly prominent in the lower energy bands (Devasia et al. 2011a; Maitra et al. 2012). At higher energies, the absorption effect is reduced, allowing emission from the polar hot spots to be significant. The similarity of the higher energy profiles in the two torque states, also observed by Beri et al. (2014), suggests the presence of a high-energy emission component with a broad pulse profile.

A correlation between the spectral parameters and the torque state of 4U 1626-67 was revealed by fitting the spectrum with the widely accepted spectral model. During the observations of the spin-up era, the time-averaged spectrum was well fitted by a blackbody temperature kT of $\sim$0.6 keV and a power law PI of $\sim$0.96. Similar spectral parameters are obtained for the source in previous spin-up states (Pravdo et al. 1979; Kii et al. 1986; Koliopanos & Gilfanov 2016; Beri et al. 2018). In the spin-down state, the PI lowered to $\sim$0.85 suggesting a hardening of the spectra, which is also observed in the earlier spin-down states. When compared to the previous spin-down state observations, we obtained a higher value of kT_{bb} although a lower value was expected. A previous study of the source using the NuSTAR observation, coinciding with our observational period, did not detect a blackbody component in their spectra (Sharma et al. 2023). Whereas, a recent study of both NuSTAR and NICER on the same observational period revealed a blackbody temperature of $\sim$0.25 keV (Tobrej et al. 2024).

The flux value obtained from our observations decreased as 4U 1626-67 went from the spin-up era to the spin-down era. A similar trend of lowering flux value is noted in the current and previous spin-down states of the source (Jain et al. 2010; Sharma et al. 2023). The luminosity of the source obtained in the spin-up state varies between $4.66 \times 10^{36}\,\mathrm{erg\,s^{-1}}$ and $5.99 \times 10^{36}\,\mathrm{erg\,s^{-1}}$. After the torque reversal, the source luminosity changed to $2.1 \times 10^{36}\,\mathrm{erg\,s^{-1}}$, indicating that the average luminosity of the source is on the order of $10^{36}\,\mathrm{erg\,s^{-1}}$. If the luminosity of the accreting pulsars is in the range $L \leqslant 10^{35-37}\,\mathrm{erg\,s^{-1}}$, then the emission pattern may be characterized by the combination of a pencil beam and a fan-beam (Kraus et al. 2003). This along with the difference in the shape of the pulse profiles and the presence and absence of QPOs can be explained by the change in the accretion flow geometry of 4U 1626-67 between spin-up and spin-down states.

Acknowledgments

This research is based on the results obtained from the AstroSat mission of the Indian Space Research Organization (ISRO), archived at the Indian Space Science Data Centre (ISSDC). This work uses data from the LAXPC instrument. We thank the LAXPC Payload Operation Center (POC) at TIFR, Mumbai, for providing the data and the necessary software tools. We thank Prof. Indulekha Kavila for her insightful comments and constructive suggestions, particularly in the discussion section of this paper. Author Juris thanks Prof. H.M. Antia for his valuable clarifications through email correspondence. Authors Juris and Marykutty acknowledge the financial support from ISRO (Sanction Order: No. *DS_2B* − 13013(2)/3/2021 − *Sec*. 2). We thank the anonymous referee for their insightful remarks and recommendations, which helped to improve this work.

References

Alpar, M. A., & Shaham, J. 1985, Natur, 316, 239
Angelini, L., White, N. E., Nagase, F., et al. 1995, ApJL, 449, L41
Antia, H. M., Yadav, J. S., Agrawal, P. C., et al. 2017, ApJS, 231, 10
Antia, H. M., Agrawal, P. C., Dedhia, D., et al. 2021, JApA, 42, 32
Basko, M. M., & Sunyaev, R. A. 1975, A&A, 42, 311
Benli, O. 2020, MNRAS, 495, 3531
Beri, A., Jain, C., Paul, B., & Raichur, H. 2014, MNRAS, 439, 1940
Beri, A., Paul, B., & Dewangan, G. C. 2018, MNRAS, 475, 999
Bildsten, L., Chakrabarty, D., Chiu, J., et al. 1997, ApJS, 113, 367
Burderi, L., Robba, N., & Cusumano, G. 1993, AdSpR, 13, 291
Camero-Arranz, A., Finger, M. H., Ikhsanov, N. R., Wilson-Hodge, C. A., & Beklen, E. 2010, ApJ, 708, 1500
Camero-Arranz, A., Pottschmidt, K., Finger, M. H., et al. 2012, A&A, 546, A40
Cannizzo, J. K. 1996, ApJL, 466, L31
Chakrabarty, D. 1998, ApJ, 492, 342
Chakrabarty, D., Homer, L., Charles, P. A., & O'Donoghue, D. 2001, ApJ, 562, 985
Chakrabarty, D., Bildsten, L., Grunsfeld, J. M., et al. 1997, ApJ, 474, 414
Deloye, C. J., Bildsten, L., & Nelemans, G. 2005, ApJ, 624, 934
Devasia, J., James, M., Paul, B., & Indulekha, K. 2011a, MNRAS, 414, 1023
Devasia, J., James, M., Paul, B., & Indulekha, K. 2011b, MNRAS, 417, 348
Giacconi, R., Murray, S., Gursky, H., et al. 1972, ApJ, 178, 281
Giles, A. B., Swank, J. H., Jahoda, K., et al. 1996, ApJL, 469, L25
Gilfanov, M., Revnivtsev, M., & Molkov, S. 2003, A&A, 410, 217
HI4PI Collaboration, Ben Bekhti, N., Flöer, L., et al. 2016, A&A, 594, A116
Iwakiri, W. B., Pottschmidt, K., Falkner, S., et al. 2019, ApJ, 878, 121
Jain, C., Paul, B., & Dutta, A. 2010, MNRAS, 403, 920
James, M., Paul, B., Devasia, J., & Indulekha, K. 2010, MNRAS, 407, 285
James, M., Paul, B., Devasia, J., & Indulekha, K. 2011, MNRAS, 410, 1489
Jenke, P., Wilson-Hodge, C., & Malacaria, C. 2023, ATel, 16011, 1
Joss, P. C., Avni, Y., & Rappaport, S. 1978, ApJ, 221, 645
Kaur, R., Paul, B., Kumar, B., & Sagar, R. 2008, ApJ, 676, 1184
Kii, T., Hayakawa, S., Nagase, F., Ikegami, T., & Kawai, N. 1986, PASJ, 38, 751
Koliopanos, F., & Gilfanov, M. 2016, MNRAS, 456, 3535
Kommers, J. M., Chakrabarty, D., & Lewin, W. H. G. 1998, ApJL, 497, L33
Kraus, U., Zahn, C., Weth, C., & Ruder, H. 2003, ApJ, 590, 424
Krauss, M. I., Schulz, N. S., Chakrabarty, D., Juett, A. M., & Cottam, J. 2007, ApJ, 660, 605
Levine, A., Ma, C. P., McClintock, J., et al. 1988, ApJ, 327, 732
Li, X. D., & van den Heuvel, E. P. J. 1997, A&A, 321, L25
Lightman, A. P., & Eardley, D. M. 1974, ApJL, 187, L1
Maitra, C., Paul, B., & Naik, S. 2012, MNRAS, 420, 2307
Manikantan, H., Paul, B., Sharma, R., Pradhan, P., & Rana, V. 2024, MNRAS, 531, 530
McClintock, J. E., Canizares, C. R., Li, F. K., & Grindlay, J. E. 1980, ApJL, 235, L81
Meszaros, P. 1992, High-energy Radiation from Magnetized Neutron Stars (Chicago, IL: Univ. Chicago Press)
Moon, D.-S., & Eikenberry, S. S. 2001, ApJL, 549, L225
Moon, D.-S., Eikenberry, S. S., & Wasserman, I. M. 2003a, ApJL, 582, L91
Moon, D.-S., Eikenberry, S. S., & Wasserman, I. M. 2003b, ApJ, 586, 1280
Mukerjee, K., & Antia, H. M. 2021, ApJ, 920, 139
Mukherjee, A., & Bhattacharyya, S. 2012, ApJ, 756, 55
Orlandini, M., Dal Fiume, D., Frontera, F., et al. 1998, ApJL, 500, L163
Paczynski, B., & Sienkiewicz, R. 1981, ApJL, 248, L27
Perna, R., Bozzo, E., & Stella, L. 2006, ApJ, 639, 363
Pravdo, S. H., White, N. E., Boldt, E. A., et al. 1979, ApJ, 231, 912
Raichur, H., & Paul, B. 2008, ApJ, 685, 1109
Raman, G., Paul, B., Bhattacharya, D., & Mohan, V. 2016, MNRAS, 458, 1302
Rappaport, S., Markert, T., Li, F. K., et al. 1977, ApJL, 217, L29
Rea, N., Israel, G. L., Di Salvo, T., Burderi, L., & Cocozza, G. 2004, A&A, 421, 235
Schulz, N. S., Chakrabarty, D., & Marshall, H. L. 2019, arXiv:1911.11684
Sharma, R., Jain, C., & Paul, B. 2023, MNRAS, 526, L35
Shinoda, K., Kii, T., Mitsuda, K., et al. 1990, PASJ, 42, L27
Singh, K. P., Tandon, S. N., Agrawal, P. C., et al. 2014, Proc. SPIE, 9144, 91441S
Tobrej, M., Tamang, R., Rai, B., Ghising, M., & Paul, B. C. 2024, MNRAS, 528, 3550
Tutukov, A. V., & Yungel'Son, L. R. 1993, ARep, 37, 411
van Kerkwijk, M. H., Chakrabarty, D., Pringle, J. E., & Wijers, R. A. M. J. 1998, ApJL, 499, L27
White, N. E., Swank, J. H., & Holt, S. S. 1983, ApJ, 270, 711
Yadav, J. S., Agrawal, P. C., Antia, H. M., et al. 2016, Proc. SPIE, 9905, 99051D